INDOOR MULTI-PERSON TRACKING VIA ULTRA-WIDEBAND RADARS

A THESIS

SUBMITTED TO THE DEPARTMENT OF ELECTRICAL AND

ELECTRONICS ENGINEERING

AND THE GRADUATE SCHOOL OF ENGINEERING AND SCIENCE

OF BILKENT UNIVERSITY

IN PARTIAL FULFILLMENT OF THE REQUIREMENTS

FOR THE DEGREE OF

MASTER OF SCIENCE

By

Berk Gülmezoğlu

August 2014

I certify that I have read this thesis and that in my opinion it is fully adequate, in scope and in quality, as a thesis for the degree of Master of Science.

Assoc. Prof. Dr. Sinan Gezici (Advisor)

I certify that I have read this thesis and that in my opinion it is fully adequate, in scope and in quality, as a thesis for the degree of Master of Science.

Assist. Prof. Dr. Mehmet Burak Güldoğan (Co-Advisor)

I certify that I have read this thesis and that in my opinion it is fully adequate, in scope and in quality, as a thesis for the degree of Master of Science.

Prof. Dr. Ahmet Enis Çetin

I certify that I have read this thesis and that in my opinion it is fully adequate, in scope and in quality, as a thesis for the degree of Master of Science.

Assoc. Prof. Dr. Çağatay Candan

Approved for the Graduate School of Engineering and Science:

Prof. Dr. Levent Onural
Director of the Graduate School

ABSTRACT

INDOOR MULTI-PERSON TRACKING VIA ULTRA-WIDEBAND RADARS

Berk Gülmezoğlu
M.S. in Electrical and Electronics Engineering
Supervisor: Assoc. Prof. Dr. Sinan Gezici
Co-Supervisor: Assist. Prof. Dr. Mehmet Burak Güldoğan
August 2014

Tracking multiple objects in indoor environments has various applications such as patient monitoring and inventory tracking. In this thesis, the use of Gaussian mixture probability hypothesis density (GM-PHD) filters is investigated for multiple person tracking via ultra-wideband (UWB) radar sensors in an indoor environment. An experimental setup consisting of a network of UWB radar sensors and a high-speed computer is designed and a new detection algorithm is proposed. The results of this experimental proof-of-concept study show that it is possible to accurately track multiple targets using a UWB radar sensor network in indoor environments based on the proposed approach.

Keywords: Multiple person detection, target tracking, PHD filter, ultra-wideband, radar, passive localization.

ÖZET

ULTRA GENİŞ BANTLI RADARLAR İLE BİNA İÇİ ÇOKLU İNSAN TAKİBİ

Berk Gülmezoğlu
Elektrik ve Elektronik Mühendisliği, Yüksek Lisans
Tez Yöneticisi: Assoc. Prof. Dr. Sinan Gezici
Eş Tez Yöneticisi: Assist. Prof. Dr. Mehmet Burak Güldoğan
Ağustos 2014

Bina içi ortamlarda çoklu nesne takibinin hasta izleme ve envanter takibi gibi çeşitli uygulamaları bulunmaktadır. Bu tezde, bina içi ortamında ultra geniş bantlı radar sensörleri ile çoklu insan takibi için Gauss karışımı olasılık hipotez yoğunluğu filtrelerinin kullanımı incelenmektedir. Ultra geniş bantlı radar sensörleri ve yüksek hızlı bir bilgisayardan oluşan deney düzeneği tasarlanmakta ve yeni bir tespit algoritması sunulmaktadır. Bu deneysel kavram ispatı çalışmasının sonuçları, önerilen yaklaşıma dayanılarak ultra geniş bantlı radar sensör ağı ile bina içi ortamlarda çoklu hedeflerin hassas takibinin mümkün olduğunu göstermektedir.

Anahtar sözcükler: Çoklu insan bulma, hedef takibi, PHD filtre, ultra geniş bant, radar, pasif yer bulma.

Acknowledgement

I would like to take this time to thank TÜBİTAK for the fellowship they provided during my M.S. studies.

I would like to thank TÜRK TELEKOM for their support and for providing the experimental setup.

I would like to thank Assoc. Prof. Dr. Sinan Gezici and Assist. Prof. Dr. Mehmet Burak Güldoğan for their supervision, special guidance, suggestions, and encouragement through the development of this thesis.

Special thanks to Prof. Dr. Ahmet Enis Çetin and Assoc. Prof. Dr. Çağatay Candan for reading and commenting on the thesis.

I would like to express my special thanks to my family for their constant support, patience and sincere love.

Finally, I would like to express my thanks to all of my friends.

Contents

List of Figures

List of Tables

Chapter 1

Introduction

Wireless sensor networks (WSN) have received tremendous attention in last decade due to their critical importance in a wide variety of applications such as surveillance, and the theoretical and practical challenges they introduce [3, 4]. For indoor scenarios, ultra-wideband (UWB) sensors can be employed due to their extraordinary resolution and localization precision [5]. There are also additional advantages of UWB signals such as low power consumption, low probability of interception, and co-existence with a large number of devices [6]. For multi-sensor multi-object tracking applications, UWB is a well-suited technology. Since UWB signals are characterized by the transmission of a few nanosecond duration pulses [1, 7–9], they have very high time resolution and localization precision, which make UWB sensors an ideal equipment for short range radar sensor network applications [10, 11]. In this study, UWB radar sensors are employed for detecting and tracking multiple moving objects in an indoor environment in the context of passive localization [12–17].

Multiple target tracking is a subfield of signal processing with applications spanning many different engineering disciplines [18]. In this subfield of signal processing, the random finite set (RFS) approach is the newest development that provides a general systematic framework for multi-target systems by modeling the multi-target state as an RFS [19, 20]. The RFS approach is considered to

be a very promising alternative to handle the multi-target multi-detection association problem faced in multi-target tracking applications. The RFS approach treats the collection of individual measurements and the individual targets as a set-valued measurement and set-valued state, respectively. It is shown that the sequential estimation of multiple targets buried in clutter with association uncertainties can be formulized in a Bayesian filtering framework by modeling set-valued measurements and set-valued states as RFSs [19]. The probability hypothesis density (PHD) filter, an approximation of this theoretically optimal approach to multi-target tracking, propagates the first-order statistical moment of the RFS of states in time and avoids the combinatorial data association problem. The dimension of the PHD filtering is equal to the dimension of the single target state. Despite its advantages, the recursions of the PHD filter involve multiple integrals having no closed form solutions. There are two implementations of the PHD filter; one is using sequential Monte Carlo (SMC) method other one is using Gaussian mixtures (GM). Each implementation method has its own pros and cons [19]. GM implementation is very popular because it provides a closed form analytic solution to PHD recursions under linear Gaussian target dynamics and measurement models [19]. Moreover, contrary to SMC implementation, GM implementation provides reliable state estimates extracted from the posterior intensity in an easier and efficient way. Alternatively, SMC implementation imposes no such restrictions and has the ability of handling nonlinear target dynamics and measurement models. It can be said that SMC implementation is a more general framework for PHD recursions. On the other hand, its performance is affected by different kind of problems in reality [21–23]. Therefore, in general, GM based approach is easier, effective and more intuitive.

Multiple target tracking via UWB sensors has been considered in some studies in the literature. In [24], time of flight (ToF) information of the targets is used for tracking using PHD filters. A single scenario with targets moving in a straight line (no maneuvers) is considered, and directional horn antennas are used for powerful signal reception. Each sensor is equipped with one transmitter and two receivers, which are synchronized via a digital resonance oscillator. The blind zone problem and its solution are explained in [25] and new approaches are developed for this

problem in tracking. In [26], multiple person tracking via UWB radar sensors is performed by utilizing time variations of the channel impulse response due to the presence of people between the transmitter and the receiver. Background subtraction and constant false alarm rate (CFAR) algorithms are employed for person detection, and GM-PHD filter tracking is used for tracking. In a similar study, [27] proposes an indoor UWB person detection and ranging technique that does not require any information about the environment and exploits the temporal variations in the received signal due to the presence of a person. Finally, in [28], localization of a passive reflector based on backscattering range measurements is studied, and theoretical performance bounds are presented.

In this study, a novel approach is developed for multi-target tracking via a network of UWB radar sensors based on GM-PHD filtering. A novel detection technique is proposed for removing a significant part of the clutters, which facilitates robust localization performance. The performance of the tracking method shows that multiple targets can be tracked efficiently in an indoor environment. Although the PHD filtering approach has been considered for multi-target tracking in [24], the considered system has high cost and complexity due to the use of six experimantal systems sensors, each equipped with one transmitter and two receivers, which employ directional horn antennas. Also, a single scenario is considered with targets moving in a straight line without any maneuvers [24]. In our study, four small off-the-shelf UWB radar sensors produced by TimeDomain [2] are employed, each sensor has a single transmitter and a receiver. Scenarios containing multiple maneuvering targets are also investigated. In addition, the proposed approach does not make any specific assumptions about the environment and positions of the targets. For multiple sensors, our method decreases the amount of computation compared to similar studies such as [29–31]. To sum up, the novelty of this work is twofold; firstly we propose a new detection technique which effectively handles severe multipath. Secondly, the GM-PHD filter is successfully used in tagless multi-person tracking problem using off-the-shelf UWB radar sensor.

The remainder of the thesis is organized as follows: In Chapter II, multi-person tracking via UWB radars is presented, and the proposed detection algorithm

is explained. In Chapter III, the experimental results are examined. Finally, Chapter IV concludes the thesis by highlighting the main contributions and listing possible topics for future research.

Chapter 2

Multi-Person Tracking via UWB Radars

2.1 UWB Signals

Ultra-wideband (UWB) is an excellent signaling choice for high accuracy localization in short to medium distances due to its high time resolution [1]. It is also well-suited for short range and low data rate communications. Some of the key applications for low rate UWB communication and localization systems are summarized in Figure 2.1.

In general, a UWB signal is defined to be a signal with a fractional bandwidth of larger than 20% and/or an absolute bandwidth of at least 500 MHz. The most important feature of UWB signals is that they have a much wider frequency band than conventional signals. Therefore, certain regulations are imposed on systems transmitting UWB signals in the world and these regulations are strict for all countries [1].

The common definitions for the bandwidths of UWB signals are as follows: The difference between the upper frequency of $-10dB$ emission point (f_H) and the lower frequency of $-10dB$ emission point (f_L) represents the absolute bandwidth

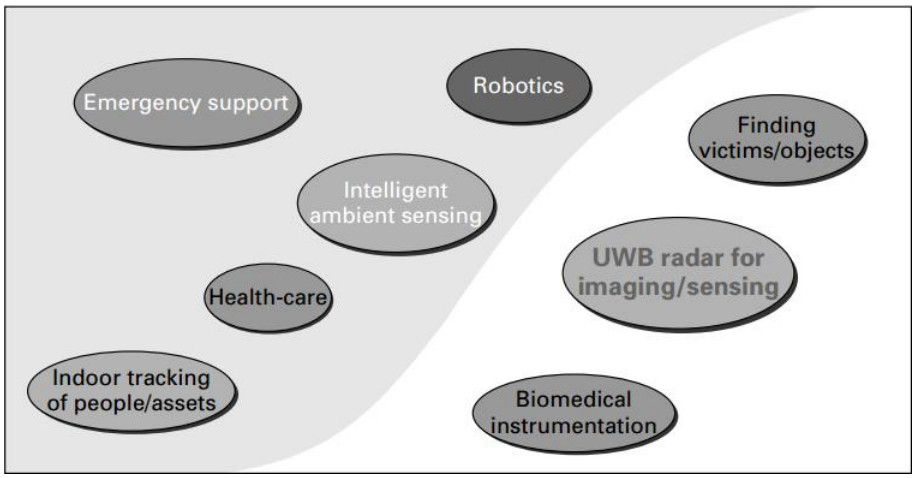

Figure 2.1: Applications and business opportunities for low rate UWB systems [1].

of the UWB signal:

$$B = f_H - f_L \ , \tag{2.1}$$

which is also named as $-10\,\mathrm{dB}$ bandwidth (Figure 2.2). On the other hand, the

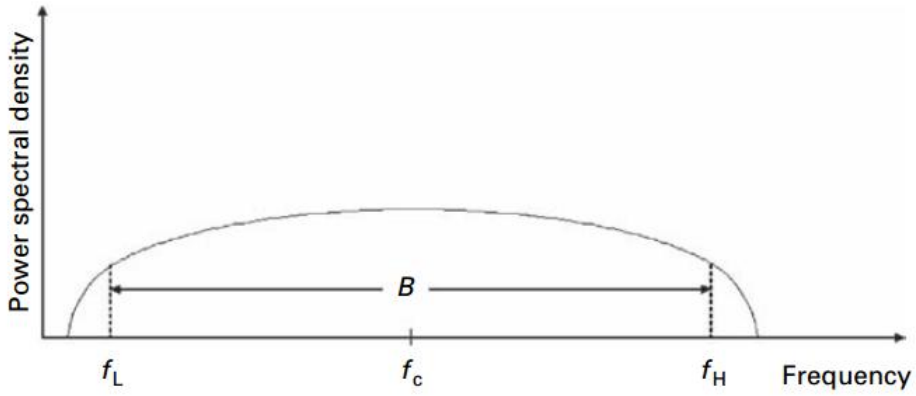

Figure 2.2: Absolute bandwidth definition [1].

fractional bandwidth is expressed as

$$B_{frac} = \frac{B}{f_c} \ , \tag{2.2}$$

where f_c is the center frequency and is given by

$$f_c = \frac{f_H + f_L}{2} \ . \tag{2.3}$$

From (2.1)-(2.3), the fractional bandwidth B_{frac} can be written as

$$B_{frac} = \frac{2(f_H - f_L)}{f_H + f_L} \ . \tag{2.4}$$

According to the U.S. FCC [32], a UWB system with f_c larger than 2.5 GHz must have an absolute bandwidth larger than 500 MHz, and a UWB system with f_c smaller than 2.5 GHz must have a fractional bandwidth larger than 0.2.

UWB systems are defined by very short duration waveforms due to their large bandwidths. Thanks to this property, UWB systems have very high time resolution, which is very useful for localization and tracking applications that require accurate position information. In this thesis, high time resolution of UWB signals is utilized in indoor tracking applications.

2.2 Sensor and Measurement Model

Before describing the sensor and measurement models, the transmitted signal model for the UWB system is given first:

$$s(t) = \sum_{j=0}^{N_{f-1}} \sum_{i=1}^{N_p} p(t - iT_p - jT_f) \tag{2.5}$$

where $p(t)$ represents the UWB pulse, T_f is the duration of a frame, T_p is the duration between UWB pulses in a frame (which is larger than the pulse duration), N_f is the number of frames, and N_p is the number of pulses in a frame. Signal $s(t)$ is produced by a UWB transmitter and the reflected signals are collected by a UWB receiver to determine the distances between targets and sensors in an indoor environment. In the process, time-of-arrival (ToA) parameters are estimated from the incoming signal, and distances corresponding to arriving signal paths are calculated based on ToA values [1].

In the measurement model, there are a number of (four in the experiments) UWB radar sensors, which constantly transmit signals, and the reflected signals from moving objects (in our case single/multiple people are walking in an indoor environment) are collected by each of these sensors as depicted in Figure 2.3.

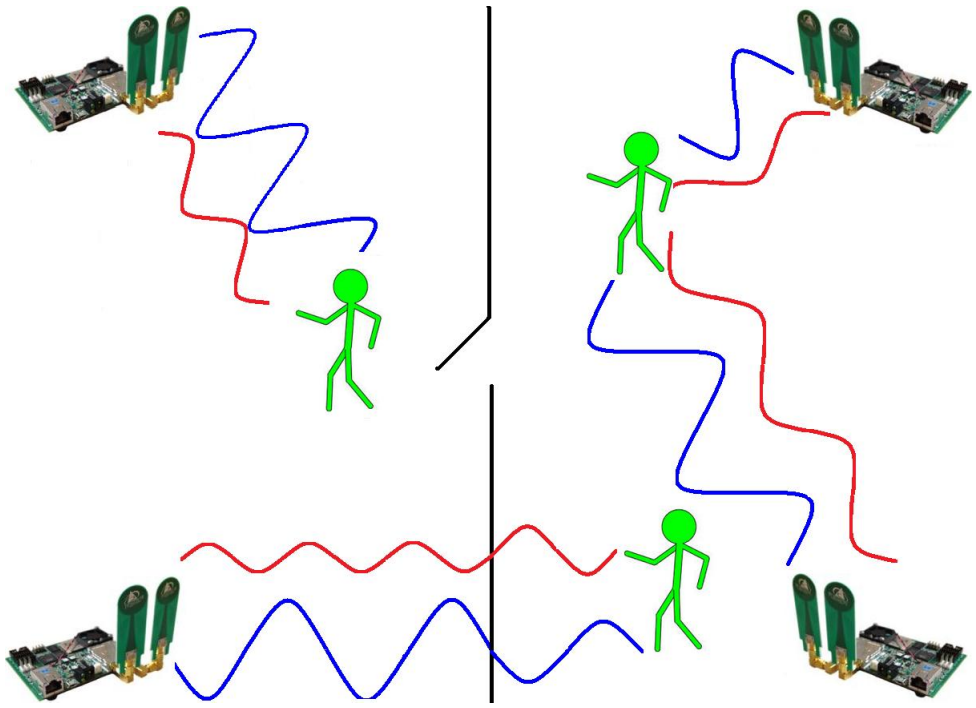

Figure 2.3: Indoor environment with four radar sensors. Blue signals and red signals represent transmitted and received signals, respectively.

The output of each sensor is the range measurements related to moving objects. It is assumed that the locations of the sensors are known to the fusion center and each sensor sends its measurements to the fusion center. The state vector of a target at time k is represented by $\mathbf{x}_k = [x_k, y_k, \dot{x}_k, \dot{y}_k]^T$, where $[x_k, y_k]$ is the position, $[\dot{x}_k, \dot{y}_k]$ is the velocity of the target and T denotes transpose operation. The target dynamic is modeled by the linear Gaussian constant velocity model [33]:

$$\mathbf{x_k} = \mathbf{F}\mathbf{x_{k-1}} + \mathbf{v_k} \tag{2.6}$$

where $\mathbf{F}$ is the state transition matrix given as,

$$\mathbf{F} = \begin{bmatrix} \mathbf{I}_2 & \triangle\mathbf{I}_2 \\ \mathbf{0}_2 & \mathbf{I}_2 \end{bmatrix} \tag{2.7}$$

and

$$\mathbf{Q} = \sigma_{\mathbf{v}}^2 \begin{bmatrix} \frac{\triangle^3}{3}\mathbf{I}_2 & \frac{\triangle^2}{2}\mathbf{I}_2 \\ \frac{\triangle^2}{2}\mathbf{I}_2 & \triangle\mathbf{I}_2 \end{bmatrix} \tag{2.8}$$

where $\mathbf{v}_k \sim \mathcal{N}(\mathbf{v}; \mathbf{0}, \mathbf{Q})$ is the white Gaussian process noise, $\mathbf{Q}$ is the covariance matrix of the process noise, $\triangle$ is the sampling interval, k is the discrete time

index, $\sigma_{\mathbf{v}}$ is the standard deviation of the process noise, and $\mathbf{I}_n$, and $\mathbf{0}_n$ denote $n \times n$ identity and zero matrices, respectively.

Range measurements are collected by each sensor in the area. The measured range value by the i-th sensor located at $[x_i, y_i]$ is given by

$$h_i(\mathbf{x}_k) = \sqrt{(x_k - x_i)^2 + (y_k - y_i)^2} + \varepsilon_{k,i} \tag{2.9}$$

for $i = 1, \ldots, N_s$, where N_s is the number of sensors and $\varepsilon_{k,i}$ is measurement noise in sensor i, $\varepsilon_{k,i} \sim \mathcal{N}(\varepsilon; 0, \sigma_\varepsilon^2)$.

We also here provide the Jacobian of $h_i(\mathbf{x}_k)$, $\mathbf{H}_{k,i}$, to be used in the filtering equations as

$$\mathbf{H}_{k,i} = \left[\begin{array}{cccc} \frac{\partial h_i(\mathbf{x}_k)}{\partial x_k} & \frac{\partial h_i(\mathbf{x}_k)}{\partial y_k} & \frac{\partial h_i(\mathbf{x}_k)}{\partial \dot{x}_k} & \frac{\partial h_i(\mathbf{x}_k)}{\partial \dot{y}_k} \end{array} \right] \tag{2.10}$$

and each of its elements are

$$\frac{\partial h_i(\mathbf{x}_k)}{\partial x_k} = \frac{x_k - x_i}{\sqrt{(x_k - x_i)^2 + (y_k - y_i)^2}} \tag{2.11}$$

$$\frac{\partial h_i(\mathbf{x}_k)}{\partial y_k} = \frac{y_k - y_i}{\sqrt{(x_k - x_i)^2 + (y_k - y_i)^2}} \tag{2.12}$$

$$\frac{\partial h_i(\mathbf{x}_k)}{\partial \dot{x}_k} = 0 \tag{2.13}$$

$$\frac{\partial h_i(\mathbf{y}_k)}{\partial \dot{y}_k} = 0 \tag{2.14}$$

2.3 Random Finite Sets (RFS) Based Filtering

The RFS framework for multiple target tracking proposed by Mahler combines the problems of combinatorial data association, detection, classification and target tracking within a unified compact Bayesian paradigm [19]. In the following

subsections, basic RFS notation, multiple target generalization of the Bayes filter and its first order approximation PHD filter are described.

2.3.1 RFS Formulation

The RFS approach treats the collection of the individual targets and individual measurements as a set-valued state and set-valued measurement, respectively, as

$$X_k = \{\mathbf{x}_{k,1}, ..., \mathbf{x}_{k,M(k)}\} \quad \in \quad \mathcal{F}(\mathcal{X}) \tag{2.15}$$

$$Z_k = \{z_{k,1}, ..., z_{k,N(k)}\} \quad \in \quad \mathcal{F}(\mathcal{Z}) \tag{2.16}$$

where $M(k)$ is the number of targets at time k, $N(k)$ is the number of measurements at time k, $\mathcal{F}(\mathcal{X})$ and $\mathcal{F}(\mathcal{Z})$ are the set of all possible finite subsets of state space $\mathcal{X}$ and measurement space $\mathcal{Z}$, respectively. An RFS model for the time evolution of a multi-target state X_{k-1} at time $k-1$ to the multi-target state X_k at time k is defined as

$$X_k = \left[\bigcup_{\boldsymbol{\zeta} \in X_{k-1}} S_{k|k-1}(\boldsymbol{\zeta}) \right] \cup \Gamma_k \quad , \tag{2.17}$$

where $S_{k|k-1}(\boldsymbol{\zeta})$ is the RFS of surviving targets from previous state $\boldsymbol{\zeta}$ at time k and Γ_k is the RFS of spontaneous target births at time k. The RFS measurement model for a multi-target state X_k at time k can be written as

$$Z_k = K_k \cup \left[\bigcup_{\mathbf{x} \in X_k} \Theta_k(\mathbf{x}) \right] \tag{2.18}$$

where K_k is the RFS of clutter or false measurements, $\Theta_k(\mathbf{x})$ is the RFS of multi-target state originated measurements, which can take values either z_k if target is detected, or $\emptyset$ if target is not detected.

2.3.2 Multi-target Filtering

Having very briefly summarized some key points of the RFS framework, we can define the RFS based multi-target Bayes filter. The optimal multi-target Bayes

filter propagates the multi-target posterior density $p_k(\cdot|Z_{1:k})$ conditioned on the sets of measurements up to time k, $Z_{1:k}$, in time with the following recursion

$$p_{k|k-1}(X_k|Z_{1:k-1}) = \int f_{k|k-1}(X_k|X)p_{k-1}(X|Z_{1:k-1})\delta X \quad , \tag{2.19}$$

$$p_k(X_k|Z_{1:k}) = \frac{g_k(Z_k|X_k)p_{k|k-1}(X_k|Z_{1:k-1})}{\int g_k(Z_k|X)p_{k|k-1}(X|Z_{1:k-1})\delta X} \quad , \tag{2.20}$$

where $f_{k|k-1}$ is the multi-target transition density, $g_k(Z_k|X_k)$ is the multi-target likelihood and integrals are set integrals defined in [19]. The multi-target Bayes recursion involves multiple integrals and the complexity of computing it grows exponentially with the number of targets. Therefore, it is not practical for scenarios where there exist more than a few targets.

2.3.3 The Probability Hypothesis Density (PHD) Filter

To alleviate the computational burden in calculating the optimal filter given above, the PHD filter was proposed as a practical suboptimal alternative [19]. The PHD filter propagates the first-order statistical moment of the posterior multi-target state, instead of propagating the multi-target posterior density. Consider that, intensities associated with the multi-target posterior density p_k and the multitarget predicted density $p_{k|k-1}$ in the optimal multi-target Bayes recursion are represented with v_k and $v_{k|k-1}$ respectively. The PHD recursion is defined as

$$v_{k|k-1}(\mathbf{x}) = \int p_s f_{k|k-1}(\mathbf{x}|\boldsymbol{\zeta})v_{k-1}(\boldsymbol{\zeta})d\boldsymbol{\zeta} + \gamma_k(\mathbf{x}) \quad , \tag{2.21}$$

$$v_k(\mathbf{x}) = (1 - p_D)v_{k|k-1}(\mathbf{x}) \tag{2.22}$$

$$+\sum_{z\in Z_k} \frac{p_D \; g_k(z|\mathbf{x}) \; v_{k|k-1}(\mathbf{x})}{\kappa_k(z) + \int p_D \; g_k(z|\boldsymbol{\xi})v_{k|k-1}(\boldsymbol{\xi})d\boldsymbol{\xi}} \quad , \tag{2.23}$$

where p_s is the probability of target survival, $\gamma_k(\mathbf{x})$ is the intensity of spontaneous birth RFS at time k, p_D is the probability of target detection and $\kappa_k(z)$ is the intensity of clutter RFS at time k.

As we mentioned before, PHD filters can be implemented either by using GM [34] or SMC [35–37] based methods. In the next section, we describe main steps of the GM implementation.

2.4 The Gaussian Mixture PHD (GM-PHD) Filter

Vo et al. derived a closed-form solution to the PHD filter, called as the GM-PHD under linear Gaussian multi-target models in [34]. The GM-PHD filter has been successfully used in many different applications [38–44]. Here, it is important to note that, in these applications target models are nonlinear. In order to accommodate nonlinear Gaussian models, an adaptation of the GM-PHD filter (called as EK-PHD) is provided based on the idea of extended Kalman (EKF) filter, where local linearizations of the nonlinear measurement function $h(\mathbf{x})$ (i.e. $\mathbf{H}_k$ defined in (2.10)) is used [34]. In this work, we used the mentioned adaptation to handle nonlinearities in measurement model in (2.9).

There are several assumptions used in the GM-PHD recursions. The first one is that each target follows a linear Gaussian dynamical and measurement model:

$$f_{k|k-1}(\mathbf{x}|\boldsymbol{\zeta}) = \mathcal{N}(\mathbf{x}; \mathbf{F}\boldsymbol{\zeta}, \mathbf{Q}_{k-1}) \ , \tag{2.24}$$

$$g_k(z|\mathbf{x}) = \mathcal{N}(z; \mathbf{H}_k\mathbf{x}, \sigma_\varepsilon^2) \ . \tag{2.25}$$

Secondly, the detection and survival probabilities are state and time independent: $p_{D,k}(\mathbf{x}) = p_D$ and $p_S(\mathbf{x}) = p_S$. Lastly, the intensity of the birth RFSs is Gaussian mixtures of the form

$$\gamma_k(x) = \sum_{i=1}^{J_{\gamma,k}} w_{\gamma,k}^{(i)} \mathcal{N}(\mathbf{x}; \mathbf{m}_{\gamma,k}^{(i)}, \mathbf{P}_{\gamma,k}^{(i)}) \ , \tag{2.26}$$

where $J_{\gamma,k}$, $w_{\gamma,k}^{(i)}$, $\mathbf{m}_{\gamma,k}^{(i)}$ and $\mathbf{P}_{\gamma,k}^{(i)}$ are given model parameters that determine the birth intensity. Posterior intensity at time $k-1$ can be written as a sum of

Gaussian components with different weights, means and covariances as

$$v_{k-1}(\mathbf{x}) = \sum_{i=1}^{J_{k-1}} w_{k-1}^{(i)} \mathcal{N}(\mathbf{x}; \mathbf{m}_{k-1}^{(i)}, \mathbf{P}_{k-1}^{(i)}) \tag{2.27}$$

and an identifying label ℓ_{k-1}^{i} is assigned to each created Gaussian component. A label table, $\mathcal{L}_{k-1}$, is formed as

$$\mathcal{L}_{k-1} = \{\ell_{k-1}^{(1)}, ..., \ell_{k-1}^{(J_{k-1})}\} \quad . \tag{2.28}$$

At time k, the predicted intensity is also a Gaussian mixture:

$$v_{k|k-1}(\mathbf{x}) = v_{S,k|k-1}(\mathbf{x}) + \gamma_k(\mathbf{x}) \quad , \tag{2.29}$$

where

$$v_{S,k|k-1}(\mathbf{x}) = p_S \sum_{j=1}^{J_{k-1}} w_{k-1}^{(j)} \mathcal{N}(\mathbf{x}; \mathbf{m}_{S,k|k-1}^{(j)}, \mathbf{P}_{S,k|k-1}^{(j)}) \tag{2.30}$$

$$\mathbf{m}_{S,k|k-1}^{(j)} = \mathbf{F}\mathbf{m}_{k-1}^{(j)} \tag{2.31}$$

$$\mathbf{P}_{S,k|k-1}^{(j)} = \mathbf{Q}_{k-1} + \mathbf{F}\mathbf{P}_{k-1}^{(j)}\mathbf{F}^T \tag{2.32}$$

Each birth component is assigned a new label and concatenated with the previous time labels,

$$\mathcal{L}_{k|k-1} = \mathcal{L}_{k-1} \cup \mathcal{L}_{\gamma,k-1} \quad . \tag{2.33}$$

The posterior intensity at time k is also a Gaussian mixture and can be written as

$$v_k(\mathbf{x}) = (1 - p_{D,k}) v_{k|k-1}(\mathbf{x}) + \sum_{z \in Z_k} v_{D,k}(\mathbf{x}; z) \quad , \tag{2.34}$$

where

$$v_{D,k}(\mathbf{x}; z) = \sum_{j=1}^{J_{k|k-1}} w_k^{(j)}(z) \mathcal{N}(\mathbf{x}; \mathbf{m}_{k|k}^{(j)}(z), \mathbf{P}_{k|k}^{(j)}) \tag{2.35}$$

$$w_k^{(j)}(z) = \frac{p_D \; w_{k|k-1}^{(j)} q_k^{(j)}(z)}{\kappa_k(z) + p_D \sum_{l=1}^{J_{k|k-1}} w_{k|k-1}^{(l)} q_k^{l}(z)} \tag{2.36}$$

$$q_k^j(z) = \mathcal{N}(z; \mathbf{H}_k \mathbf{m}_{k|k-1}^{(j)}, \sigma_\varepsilon^2 + \mathbf{H}_k \mathbf{P}_{k|k-1}^{(j)} \mathbf{H}_k^T) \tag{2.37}$$

$$\mathbf{m}_{k|k}^{(j)}(z) = \mathbf{m}_{k|k-1}^{(j)} + \mathbf{K}_k^{(j)}(z - \mathbf{H}_k \mathbf{m}_{k|k-1}^{(j)}) \tag{2.38}$$

$$P_{k|k}^{(j)} = [\mathbf{I} - \mathbf{K}_k^{(j)} \mathbf{H}_k] \mathbf{P}_{k|k-1}^{(j)} \tag{2.39}$$

$$\mathbf{K}_k^{(j)} = \mathbf{P}_{k|k-1}^{(j)} \mathbf{H}_k^T (\mathbf{H}_k \mathbf{P}_{k|k-1}^{(j)} \mathbf{H}_k^T + \sigma_\varepsilon^2)^{-1} \tag{2.40}$$

There will be $|Z_k|+1$ Gaussian components for each predicted term, where $|\cdot|$ is the cardinality of a set. Then, identifying label at time k is

$$\mathcal{L}_k = \mathcal{L}_{k|k-1}^{v_{k|k-1}} \cup \mathcal{L}_{k|k-1}^{z_1} \cup ... \cup \mathcal{L}_{k|k-1}^{z_{|Z_k|}} \quad . \tag{2.41}$$

As time progresses, the number of Gaussian components increases and computational problems occur. To alleviate this problem, a simple pruning and merging can be used to decrease the number of Gaussian components propagated [34]. Firstly, weights below a predefined threshold are eliminated. Then, closely spaced Gaussian components are merged into a single Gaussian component. Starting with the strongest weighted component, w_k^j, components are merged in a set $W_k^{(j)}$ by

$$W_k^{(j)} := \left\{ i : \ (\mathbf{m}_k^{(i)} - \mathbf{m}_k^{(j)})^T (\mathbf{P}_k^{(i)})^{-1} (\mathbf{m}_k^{(i)} - \mathbf{m}_k^{(j)}) \leq \rho \right\} \tag{2.42}$$

and the resulting merged component parameters are

$$\tilde{w}_k^{(l)} = \sum_{i \in W} w_k^{(i)} \tag{2.43}$$

$$\tilde{\mathbf{m}}_k^{(l)} = \frac{1}{\tilde{w}_k^{(l)}} \sum_{i \in W} w_k^{(i)} \mathbf{x}_k^{(i)} \tag{2.44}$$

$$\tilde{\mathbf{P}}_k^{(l)} = \frac{1}{\tilde{w}_k^{(l)}} \sum_{i \in W} w_k^{(i)} (\mathbf{P}_k^{(i)} + (\tilde{\mathbf{m}}_k^{(l)} - \mathbf{m}_k^{(i)})(\tilde{\mathbf{m}}_k^{(l)} - \mathbf{m}_k^{(i)})^T) \tag{2.45}$$

In order to extract multi-target states, means of the Gaussian components, that have weights greater than some predefined threshold, are selected:

$$\hat{\mathcal{L}}_k = \left\{ \mathcal{L}_k^{(i)} : w_k^{(i)} > \rho \right\} \quad , \tag{2.46}$$

and the estimated target states set is

$$\hat{X}_k = \left\{ (\mathbf{m}_k^{(i)}, \mathbf{P}_k^{(i)}) : \mathcal{L}_k^{(i)} \in \hat{\mathcal{L}}_k \right\} \quad . \tag{2.47}$$

2.5 UWB Radar Sensors

In this part, some technical details of the Pulson 410 Monostatic Radar Module (P410 MRM) are presented [2]. P410 MRM is a monostatic radar platform that

employs UWB signals. Based on the operator instruction, the MRM Service can perform band-pass filtering, motion filtering, and constant false alarm rate (CFAR) target detection on the raw scan data. The processed data is provided to the MRM reconfiguration and evaluation tool (RET) for display and logging. The user has the option of applying several different types of filters. A system block diagram is shown in Figure 2.4.

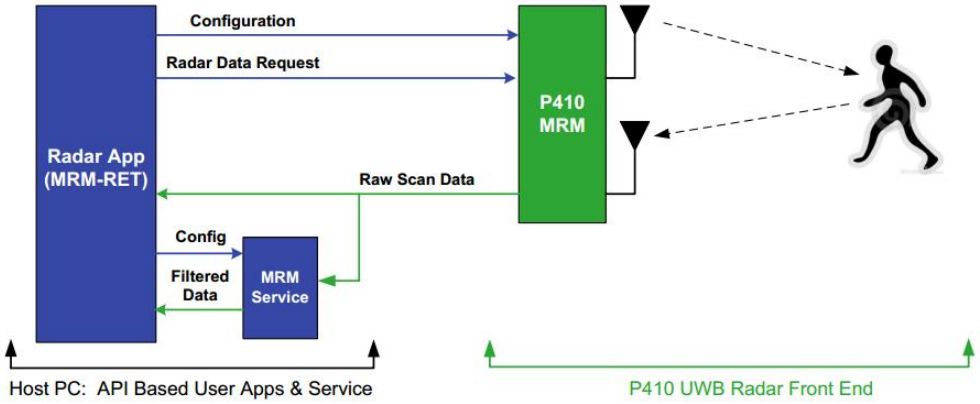

Figure 2.4: Illustration of the interface to a P410 MRM [2].

There are some advantages of the P410 MRM such as very good performance in high multipath and high clutter environments, coherent signal processing (which extends the operating range at very low signal power levels), and the availability of seven separate channels. Moreover, the P410 MRM provides raw scans for post processing and two user-configurable antenna ports for dual antenna operation. At the same time, there are some other application areas such as robotics, proximity detection, collision avoidance, security applications, presence/intrusion detection and surveillance [2].

Using the P410 MRM is quite simple. First, all the sensors should be connected to a computer. For this purpose, the IP addresses of the specific P410 MRMs are entered to the Network IP Address as illustrated in Figure 2.5. After connecting the sensors (P410 MRMs) to the computer, the configuration menu is started (Figure 2.6). In this window, the sensor parameters are tuned. Especially, the code channel has a significant role for multi-sensor operations; namely, in order to prevent the collisions among sensors' signals, the channel codes should

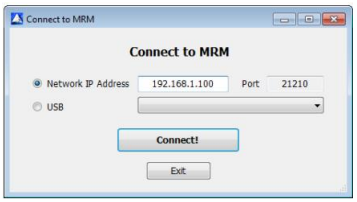

Figure 2.5: P410 MRM with attached broadspec antennas [2].

be different for each sensor. Moreover, the scan start and stop times provide the sensors with the facility to scan the environment so that the locations of the fixed equipments in the environment can be known by the sensors. The second user

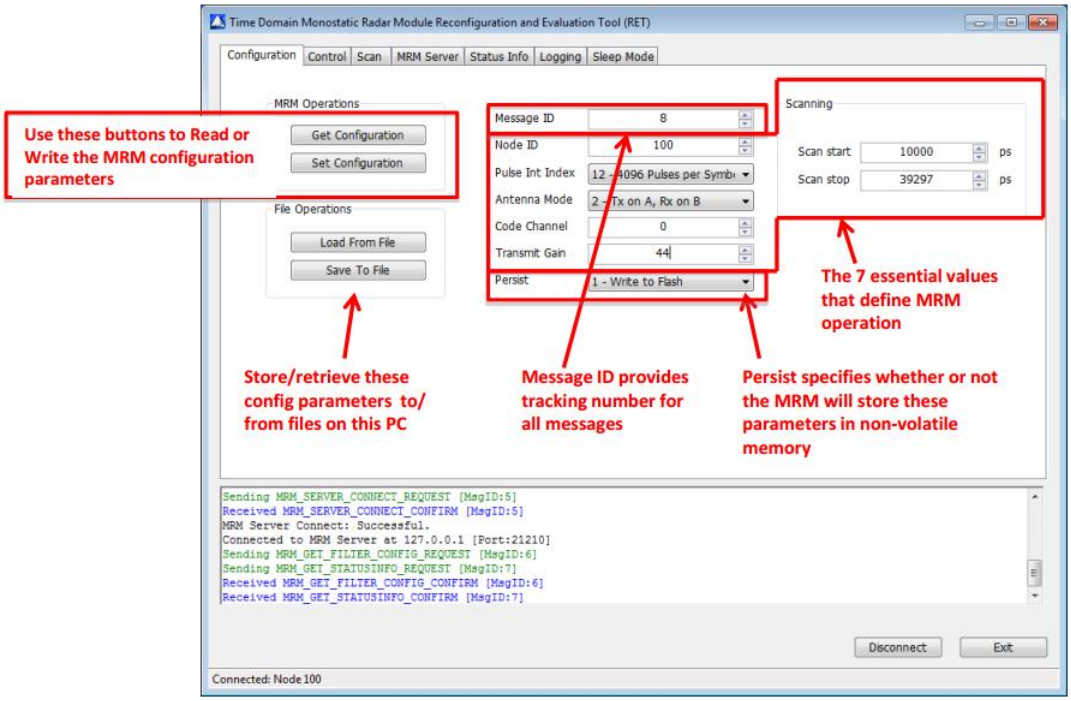

Figure 2.6: Configuration window [2].

interface window is about the scanning of the sensors (Figure 2.7). The time between consecutive two impulses is adjusted by the interval section. In addition, the impulse number can be constant depending on the request of user or it can be continuous until the user stops. The last important part of the software for the P410 MRM is the scan window (Figure 2.8). In this window, all data types can be seen such as raw, bandpass, and motion filtered data. Moreover, detection points and the first detection points can be observed.

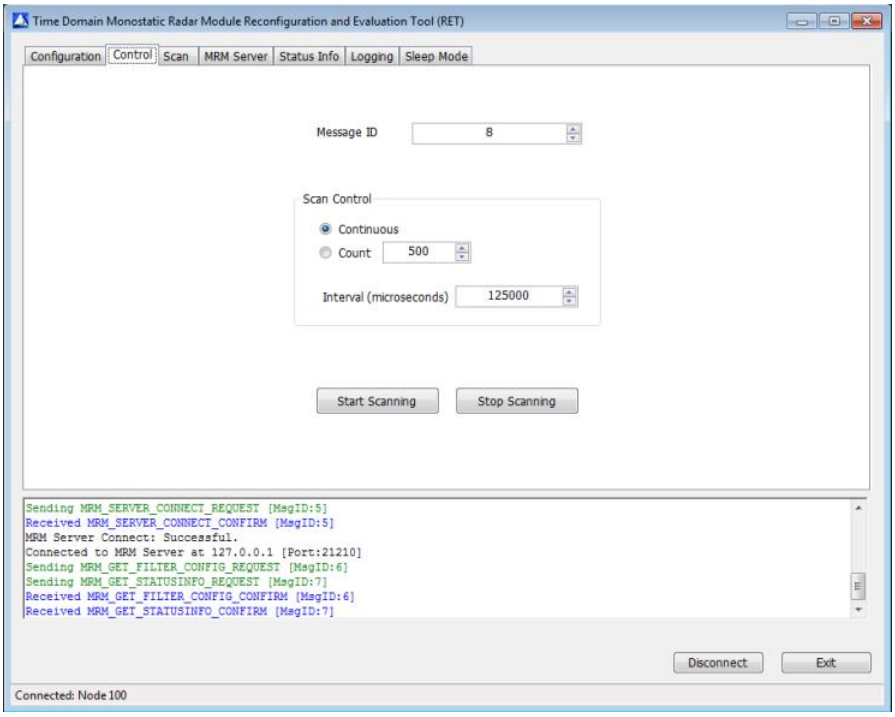

Figure 2.7: Control window [2].

In our experiments, four P410 MRMs are employed as radar sensors. The P410 MRM, shown in Figure 2.9, is a small and affordable monostatic radar platform that provides more than 2 GHz of RF bandwidth at a center frequency of 4.3 GHz [2]. Each radar sensor (P410 MRM) is equipped with an UWB transmitter and an UWB receiver. The radar sensors use different code channels in order to prevent interference among the sensors. In addition, for reducing the effects of severe multipaths at the receiver, there is an environment scanning phase for a 30 ns duration, which is used as a reference for determining signals reflected from non-stationary objects. The UWB pulses are sent from the radar sensors at every 0.1 second by the transmitter (TX) antenna and all reflected signals are collected by the receiver (RX) antenna. P410 MRM UWB sensors provide four types of information; raw signal, bandpass signal, motion filtered signal, and detection list. In some cases, the motion filtered data and detection lists may not be sufficient to detect the targets accurately since there can be many unnecessary measurements (due to the very high resolution of UWB signals) that are originated from the reflections from other equipments or objects in the environment. Therefore, we use the bandpass data (see Figure 2.10 for an example) in our algorithm in order

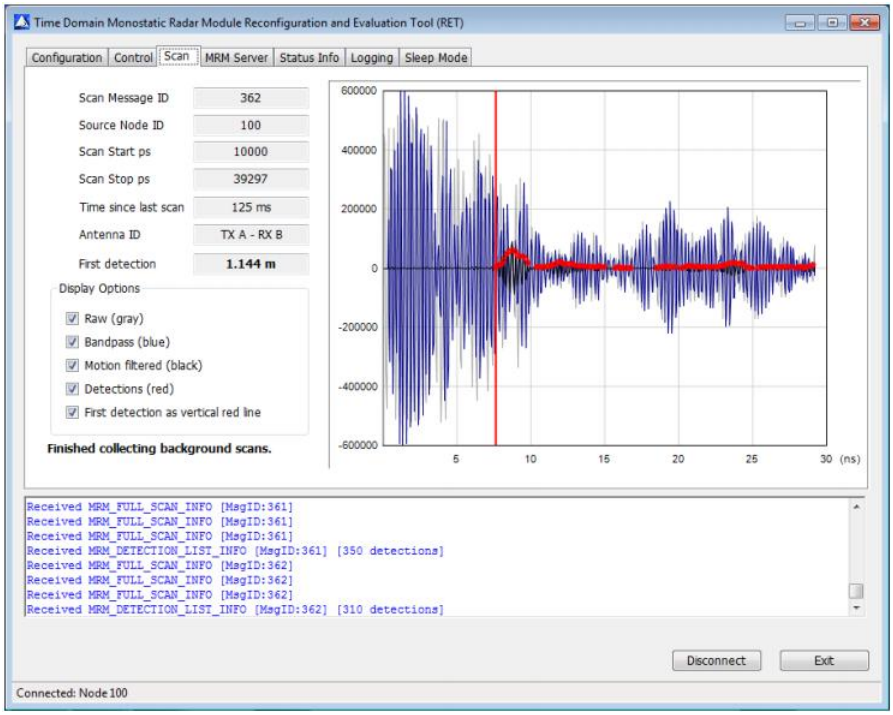

Figure 2.8: Control window [2].

to eliminate the clutters, and then obtain the motion filtered data, as explained in the next section. Fig 2.11 presents an example of motion filtered data when a person is present in the environment.

2.6 Proposed Detection/Tracking Algorithm

In order to perform accurate detection and tracking of multiple persons via UWB radar sensors, the following algorithm is proposed. The input to the algorithm is the bandpass signal sets from the UWB radar sensors. Figure 2.10 illustrates an example for bandpass signal at an arbitrary time stamp. After getting the bandpass signal sets from the radar sensors, the start time (t_s) and stop time (t_f) of the experiment are calculated. In total, N_d sets of measurements are obtained from the sensors, where N_d is given by

$$N_d = \frac{t_f - t_s}{T_s} \tag{2.48}$$

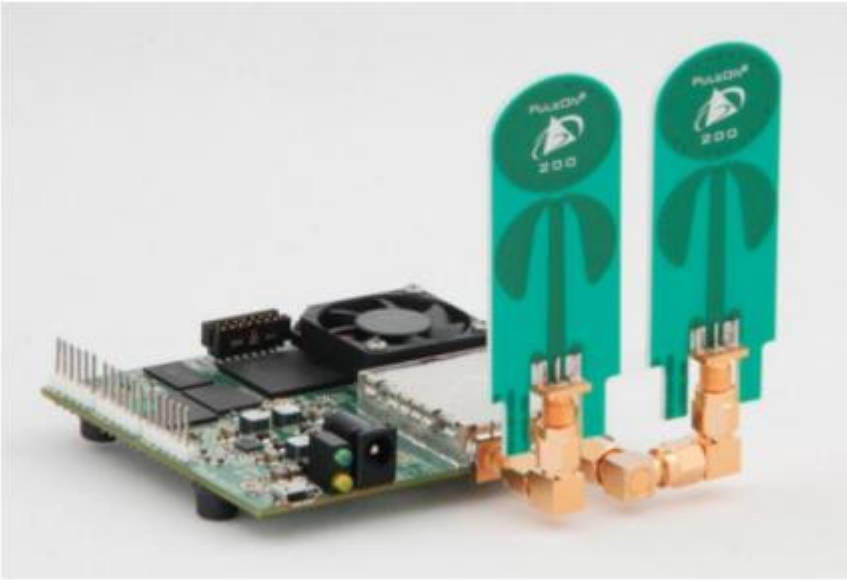

Figure 2.9: P410 MRM with attached broadspec antennas [2].

with T_s representing the sampling period of the signal set, which is equal for all sensors. The bandpass signal set is filtered by a motion filter in order to mitigate the effects of the signals coming from stationary objects in the environment. The following motion filtering method is employed:

$$\begin{aligned} m_k^i[n] = h[1]r_k^i[n] + h[2]r_k^i[n-1] \\ + h[3]r_k^i[n-2] + h[4]r_k^i[n-3] \end{aligned} \tag{2.49}$$

for $i \in \{1, \ldots, 4\}$ and $k \in \{1, \ldots, N_d\}$, where $r_k^i[n]$ represents the bandpass signal of the ith radar sensor for the kth measurement set, $h[n]$ denotes the coefficients of the motion filter with values [1 -0.6 -0.3 -0.1], and N_d is the number of measurement sets as defined in (2.48). In other words, for each measurement set and for each sensor, the motion filter in (2.49) is applied to the bandpass signal, and the motion filtered signal $m_k^i[n]$ is generated. The peaks of the motion filtered signal correspond to possible target distances as can be observed from Figure 2.11.

Next, each motion filtered signal is divided into (N_b) blocks as follows:

$$m_{k,j}^i[n] = m_k^i[n + (j-1)K], \quad n = 1, \ldots, K \tag{2.50}$$

for $j \in \{1, \ldots, N_b\}$, where K is the number of samples in each block, which

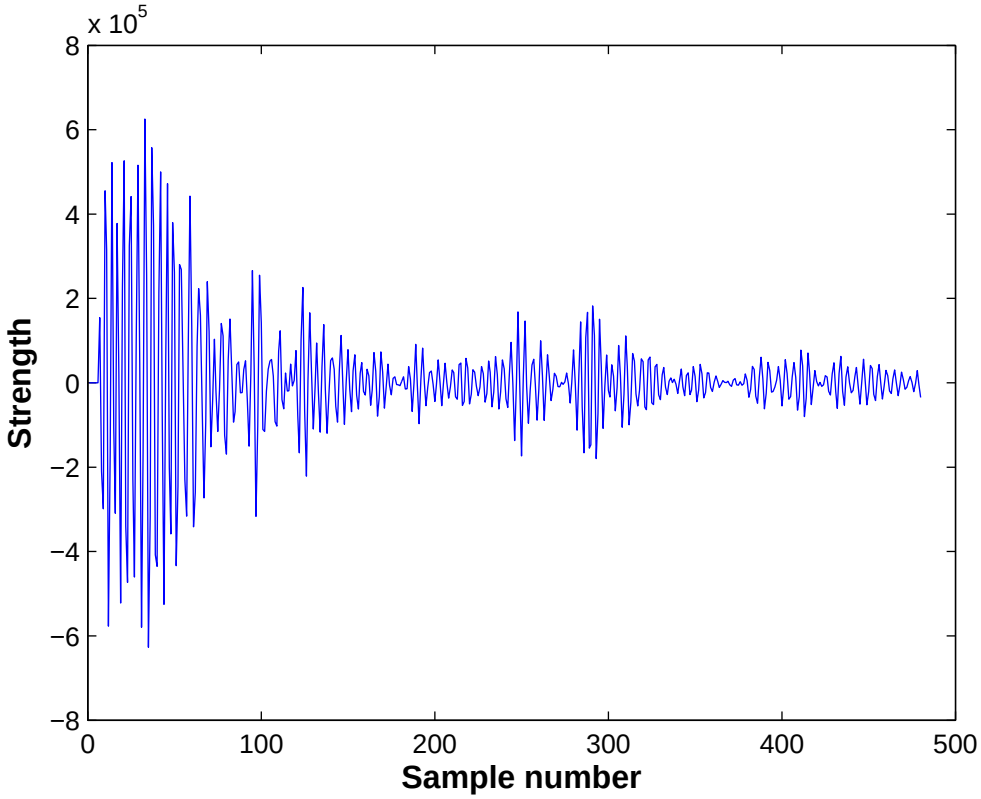

Figure 2.10: Bandpass signal.

is considered as constant.[1] An example illustration is presented in Figure 2.12, where $N_b = 5$. The aim of dividing motion filtered signal into blocks is to increase both the efficiency and the speed of the proposed algorithm, which can be justified as follows. Due to the very high time resolution of UWB signals, there exist many peaks in the motion filtered signal, most of which are originated from the same targets (that is, each moving object/person results in many peaks in the motion filtered signal). In order to determine the number of targets accurately (hence, to track them efficiently), only a few significant motion filter peaks should be considered, which is facilitated by the proposed block operation in (2.50) (and the energy thresholding technique explained below). This operation also increases the speed of the algorithm since a smaller set of measurements are input to the tracking part of the algorithm. The number of blocks, N_b, is an important

[1]For simplicity of notation, the size of signal $m_k^i[n]$ is assumed to be an integer multiple of K. Extensions in the absence of this assumption are straightforward.

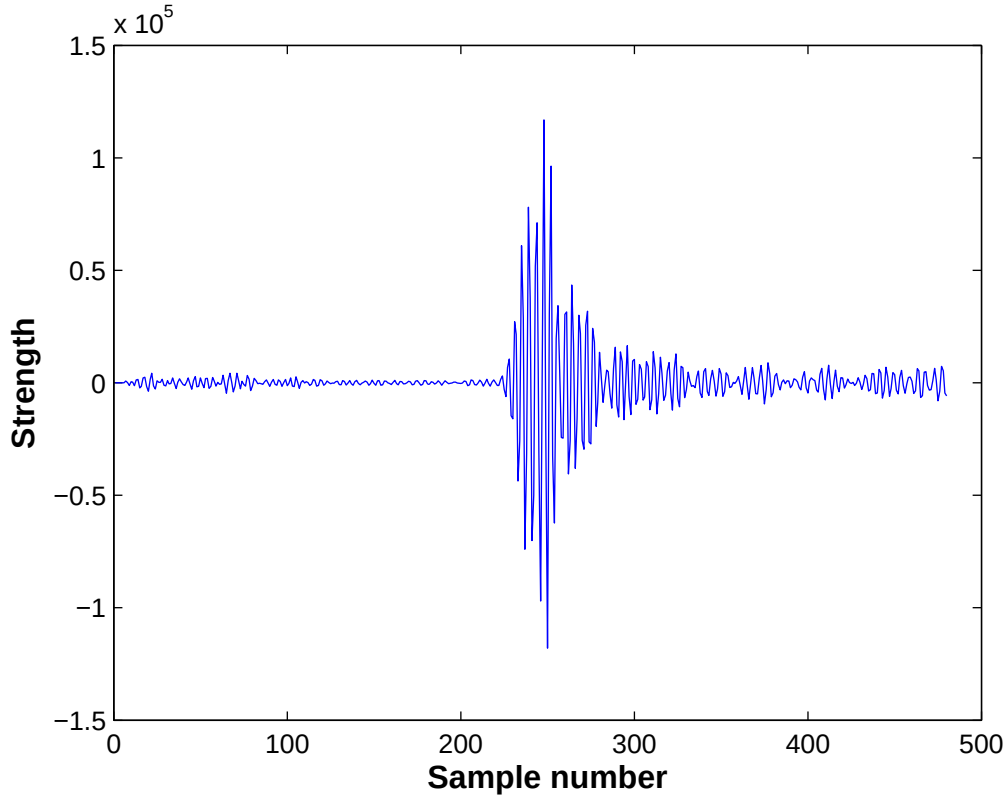

Figure 2.11: Motion filtered data.

parameter, which should be selected according to the number of expected targets in the environment. As the number of targets increases, N_b should be set to a larger number.

Once the motion filtered signal is divided into blocks, the average strength of each block is calculated as follows:

$$E^i_{k,j} \triangleq \frac{1}{K} \sum_{n=1}^{K} \left| m^i_{k,j}[n] \right| \tag{2.51}$$

for $j \in \{1, \ldots, N_b\}$, $i \in \{1, \ldots, 4\}$, and $k \in \{1, \ldots, N_d\}$. Then, these values are compared to a threshold τ_i for each sensor in order to eliminate the blocks that do not contain signals from the targets. In other words, if the average strength of a block is below the threshold, then that block is not considered in the next steps. This process both reduces the computational complexity and number of detections. If the average strength of a block is larger than the threshold, then the

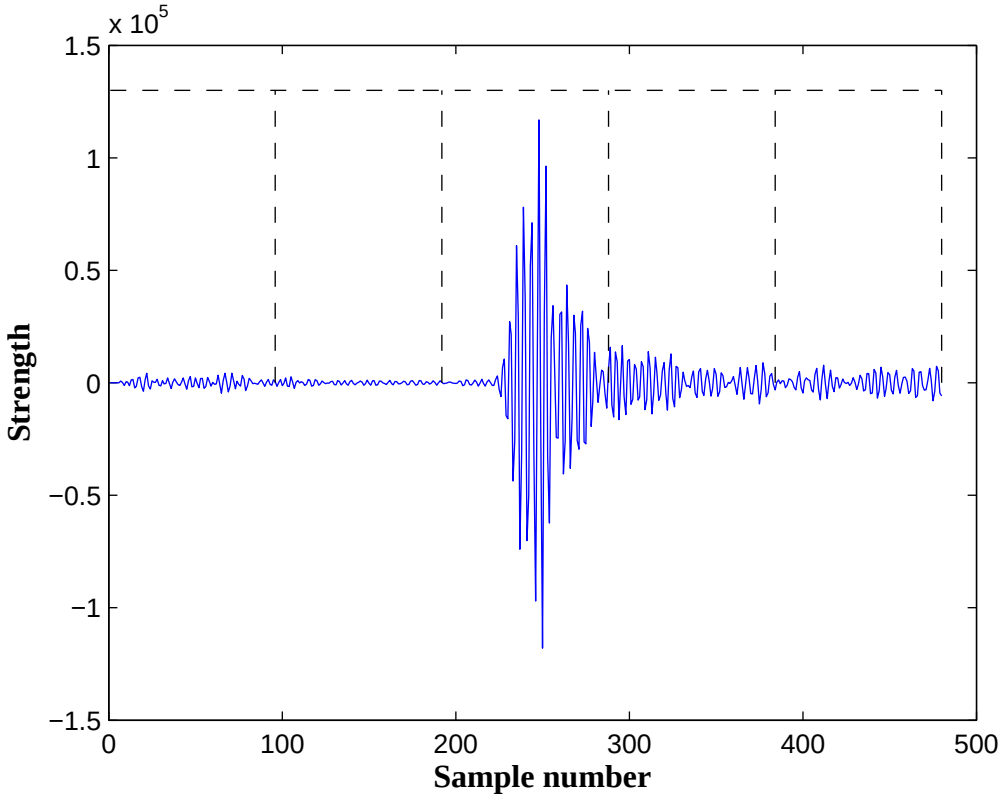

Figure 2.12: Blocks of motion filtered signal.

sample index of the strongest motion filter output in that block is converted into distance (meters) and stored into the measurement vector Z_k^i. Mathematically, for $j \in \{1, \ldots, N_b\}$, if $E_{k,j}^i > \tau_i$, then the sample index

$$\underset{n \in \{1,\ldots,K\}}{\arg\max} \left| m_{k,j}^i[n] \right| \tag{2.52}$$

is converted into distance and saved into Z_k^i. Therefore, Z_k^i is a vector with G_k^i measurements, where $G_k^i \in \{0, 1, \ldots, N_b\}$ is the number of blocks that satisfy $E_{k,j}^i > \tau_i$.[2] Measurements from all four sensors are collected into measurement set Z_k as in (2.15); that is, $Z_k = [Z_k^1; Z_k^2; Z_k^3; Z_k^4]$. Then, Z_k is input to the GM-PHD filter described in Section 2.4, and tracking is performed. The proposed detection and tracking algorithm is summarized in Table 2.1.

[2]If the strengths of all the blocks are below τ_i, then Z_k^i becomes an empty vector, $Z_k^i = \emptyset$.

Table 2.1: Proposed Algorithm

Calculate the number of measurement sets N_d, (2.48)
for $k = 1 \rightarrow N_d$ **do**
    for $i = 1 \rightarrow Q_s$ **do**
        Get bandpass signal $r_k^i[n]$ from radar sensors
        Obtain motion filtered signal $m_k^i[n]$, (2.49)
        Divide motion filtered signal into blocks as in (2.50), and obtain $m_{k,j}^i[n]$ for $j = 1, \ldots, N_b$
        for $j = 1 \rightarrow N_b$ **do**
            Calculate $E_{k,j}^i$ in (2.51)
            if $E_{k,j}^i$ is larger than threshold τ_i **then**
                Find sample index of the peak as in (2.52)
                Convert the sample index into distance
                Store the distance into Z_k^i
            end if
        end for
    end for
    Form $Z_k = [Z_k^1; Z_k^2; Z_k^3; Z_k^4]$ as in (2.15)
    Input Z_k to the GM-PHD filter (Section 2.4)
end for

Chapter 3

Experimental Results

3.1 Experimental Results

Experimental results for single and multiple person are presented in this section. The experiments are performed in an office room in the Department of Electrical and Electronics Engineering at Bilkent University. There are many equipments/objects which can generate multipaths in the office environment as seen in Fig 3.1. In the experiments, four P410 MRMs are used. In order to reduce the number of detections and the computational complexity of the algorithm, the number of blocks is set to six in the algorithm; that is, $N_b = 6$ (see (2.50)). The threshold τ_i in Section 2.6 is set to 12000 (in units of P410 MRM outputs) in order to determine and eliminate noise only blocks, and the sampling period T_s is taken as 0.1 second.

The standard deviation of the process noise is taken as $\sigma_v = 2\,\mathrm{m/s}^2$ and the standard deviation of the measurement noise is taken as $\sigma_\varepsilon = 0.2\,\mathrm{m}$. The spontaneous birth intensities are described in the center of the tracking area since the birth locations are assumed as unknown. Hence, our method can be applied to any scenario and we do not need to describe the birth intensities even though the tracking is lost. In the algorithm, the initial weights which are described in Section 2.4 as in (2.26) are taken as $w_i = 0.1$. In pruning

Figure 3.1: An illustration of the office environment. Four radar sensors are placed on the chairs.

parameters, the truncation threshold for the weights is chosen as $\rho = 10^{-6}$ and the maximum allowable number of Gaussian terms is taken as 20. In our scenario, the tracking scenario is not very complicated; hence, this number is set to 20 in order to have a faster result. However, in complex cases, this component number can be increased. In clutter distribution, we determine the highest and smallest measurements in order to estimate the number of clutters. The detected measurements are immersed in clutter that can be modelled as Poisson RFS K_k with intensity

$$\kappa_k(z) = \lambda_c V u(z) \tag{3.1}$$

where $u(\cdot)$ is the uniform density over the surveillance region, $V = 12m^2$ is the "volume" of the surveillance region, and $\lambda_c = 0.417m^{-2}$ is the average number of clutter returns per unit volume (i.e., 5 clutter returns over the surveillance region).

Our computer has 8 GB RAM and its speed is 3.40 GHz Intel(R) Core(TM)

i7. The proposed approach runs at real-time and one iteration of the experiment take approximately 1s on the average.

3.1.1 Single-Person Tracking Results

In the first set of experiments, we consider the tracking of one person and study two different scenarios. In the first scenario (Scenario-1), the person (target) starts from position $(0, 2.5)$ m. and walks in a straight line until $(2.8, 2.5)$ m. Then, he turns right and walks until $(2.8, 0.5)$ m. After that, he again turns right and goes until $(0, 0.5)$ m. The person walks with a constant speed of around 0.4 m/s, and the experiment takes about 19 seconds. The results are shown in Figure 3.2, where the blue line is the ground truth of the target path, and the red circles are the estimates of the proposed algorithm. The width of the person is about 0.5 m and at different positions reflections from different parts of the body are received. Therefore, the blue line is in fact the approximate ground truth of the person's path. For this reason, the red circles slightly digress from the blue line as expected. The differences between the blue line and the red circles are always smaller than 0.25 m in this scenario, which indicates that the positions of the person can be estimated accurately by the proposed algorithm in this case.

The second scenario (Scenario-2) for the single target case involves a more challenging target path with target maneuvers in a small area. In this scenario, the target starts to move from position $(0.6, 0.7)$ m. and comes back to the same position after following the blue path in Figure 3.3. Similar to the previous experiment, the red circles in Figure 3.3 are very close to the real path and the algorithm performs very well for this difficult scenario. Duration of the experiment is approximately 29s.

In Figure 3.4, the detection data obtained from four UWB radar sensors are illustrated for the scenario in Figure 3.3. As discussed in Section 2.6, the indices of the strongest samples are calculated for the blocks of motion filtered data that have an average value larger than the threshold. Therefore, in the figures, the number of points at each time instant indicates the number of blocks the

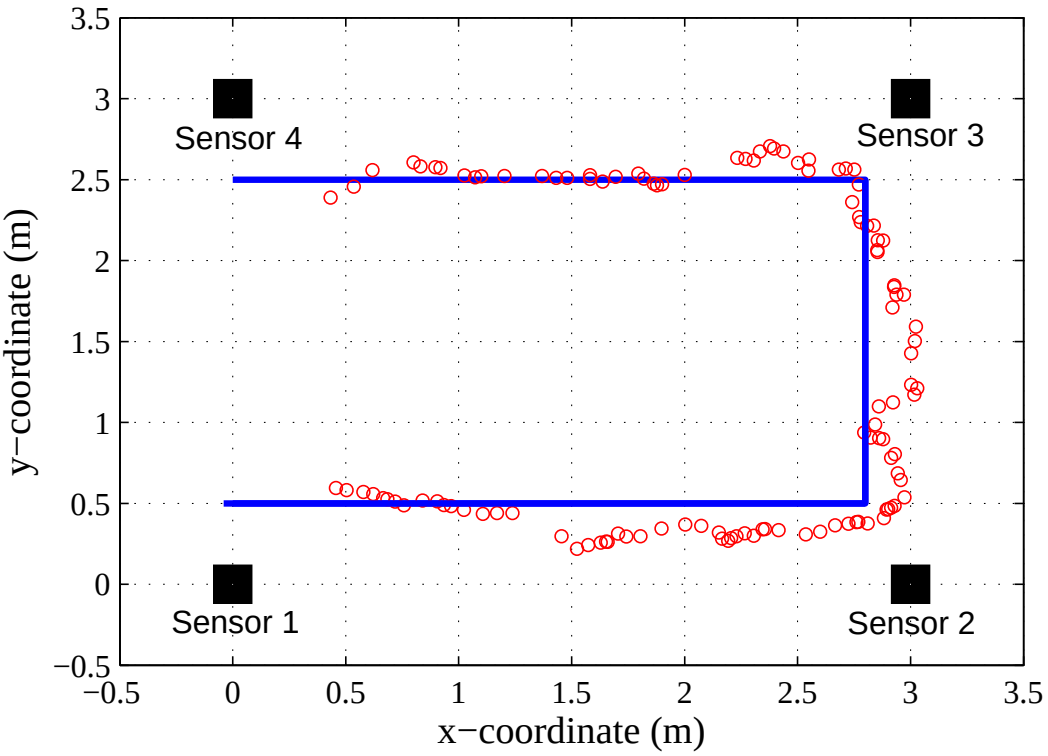

Figure 3.2: Scenario-1 for single-person tracking. Blue solid line and red circles represent the ground truth and filter estimates, respectively. Black squares are for UWB radar sensors.

average strength of which are above the threshold (equivalently, the number of elements in Z_k^i for a given time index k and sensor index i; see Section 2.6). The points in the figures are color coded in such a way that the colors blue, green, red, cyan, and magenta are employed in the order of increasing distances from the sensors; that is, the blue and purple points are used for the detection points that are closest to and furthest away from the given sensor, respectively. It is observed from Figure 3.4 that there are many non-target detections due to the high time resolution of UWB signals. However, the GM-PHD filter can successfully eliminate clutter and provide accurate tracking results, as shown Figure 3.3.

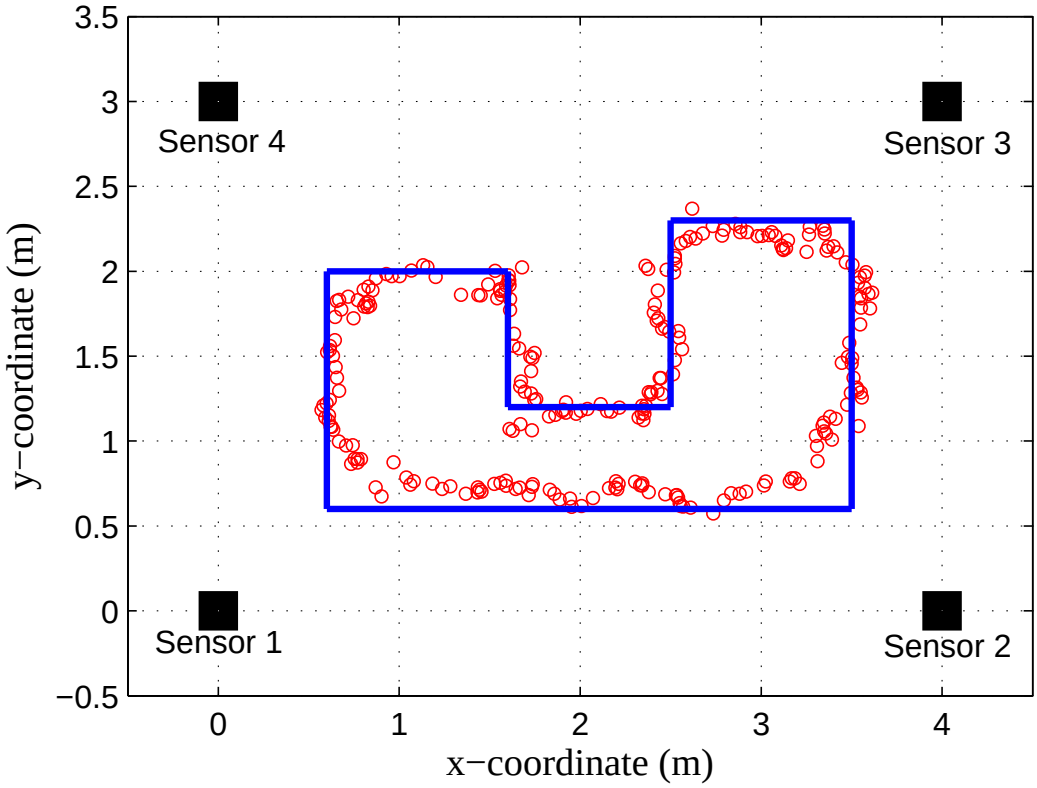

Figure 3.3: Scenario-2 for single-person tracking. Blue solid line and red circles represent the ground truth and filter estimates, respectively. Black squares are for UWB radar sensors.

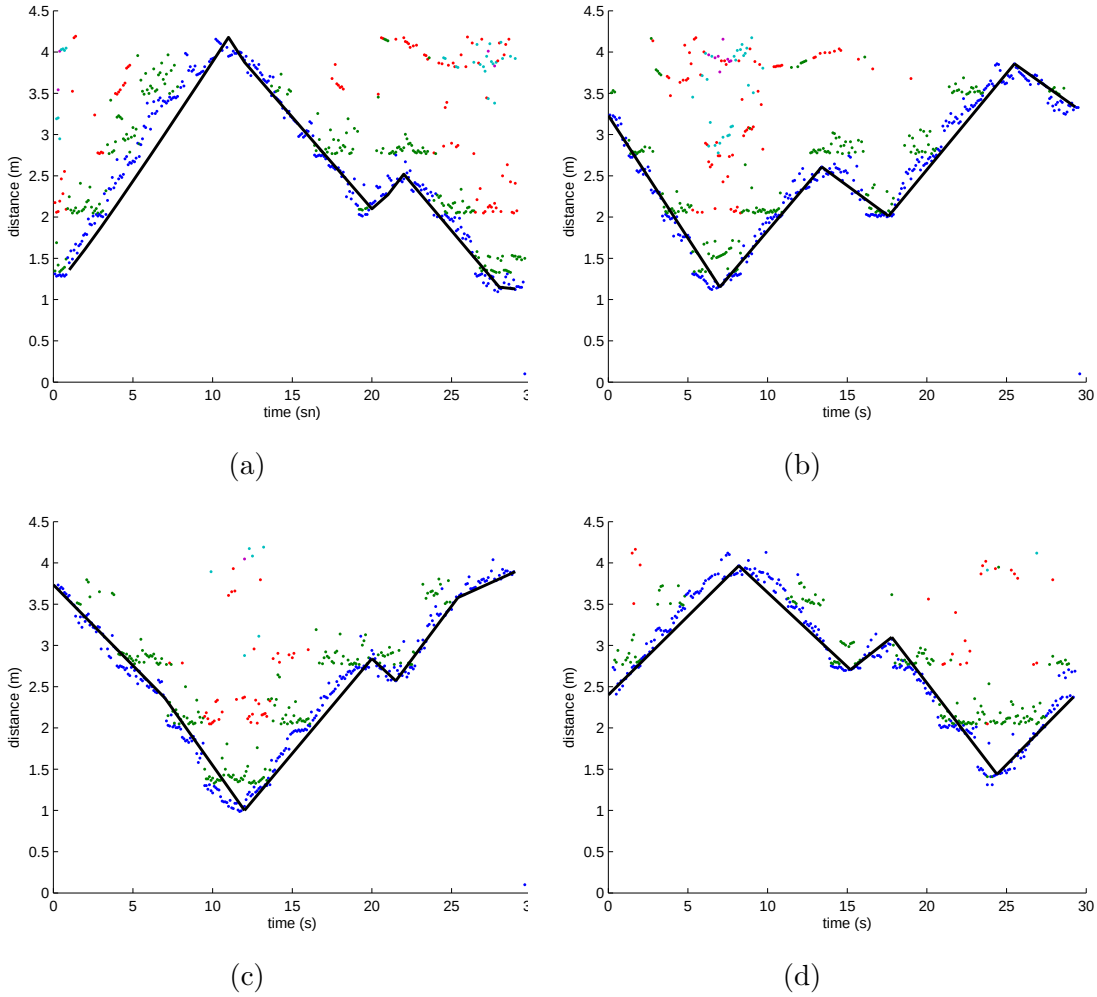

Figure 3.4: Single person tracking scenario, (Scenario-2). Range measurements of each sensor: (a) Sensor 1 (b) Sensor 2 (c) Sensor 3 (d) Sensor 4

3.1.2 Multi-Person Tracking Results

Next, we consider cases, where multiple-person are walking. First, we choose to perform controlled experiments for two people. The first person starts from the position $(3, 3)$ m. and the other person starts from the position $(0, 1.5)$ m. The first person walks until $(3, 0)$ m. and turns right. Then, he walks until $(1, 0)$ m. His speed is constant and it is about $0.3\,\mathrm{m/s}$. The second person walks in a straight line and its velocity is about $0.25\,\mathrm{m/s}$. The ground truths are shown in Figure 3.5 with the blue lines. The experiment takes about 16 seconds. In addition, the sensor locations are different from those in the previous experiments (Sensor 1 at $(0, 0)$, Sensor 2 at $(2, -1)$ m., Sensor 3 at $(4, 0)$ m., and Sensor 4 at $(2, 3)$ m., as shown in Figure 3.5). The red circles represent the estimation results and they are commonly in the range of the human body. Therefore, for the multiple person case, the algorithm performs well in this scenario. There are some differences between the single and multiple person tracking scenarios. For instance, the sensor measurements are more complicated in the multiple person case, which can be observed by comparing the sensor data in Figure 3.6 with that in Figure 3.4. In particular, when there are a larger number of detection points (represented by different colors) for a time instant, target originated detections and clutters are observed more frequently, which makes the tracking of people more challenging.

In the final experiment, our aim is to track random paths which are not defined to people before the experiment. One of the difficult scenarios is the one shown in Figure 3.7 since there is an occlusion problem as the sensors may not detect the locations of people when they are in the same line. Therefore, the occlusion problem makes the situation quite complicated. In this experiment, there are two people with the first target starting from $(0.7, 1.5)$ m. and the second person from $(3.7, 1.5)$ m. The first person goes to $(2.2, 3)$ m. and then continues to walk until $(3.7, 1.5)$ m. while the second person goes to $(2.2, 0)$ m. and then finishes his walk on $(0.7, 1.5)$ m. The red circles are the location estimates for the people. In this case, some points cannot be detected. However, most of the time, people can be tracked with high accuracy by the proposed algorithm.

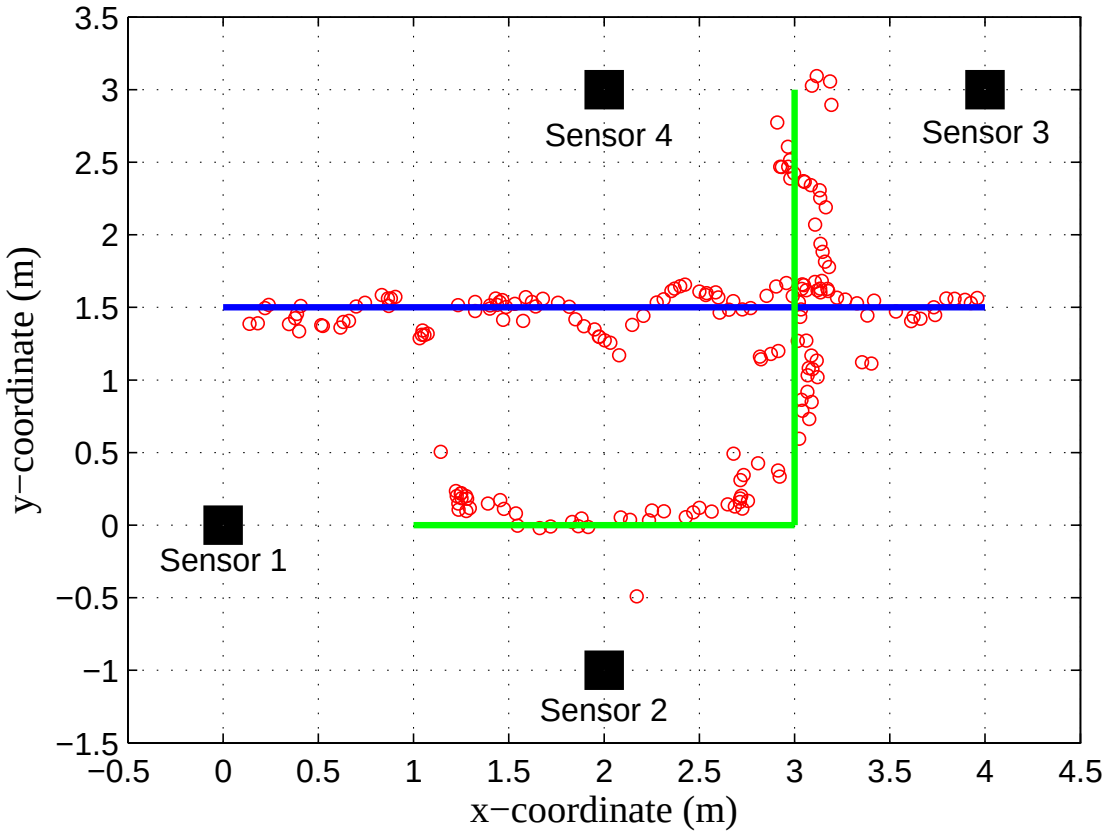

Figure 3.5: Scenario-1 for multiple person tracking. Green and blue solid lines denote the ground truth of the first and second person, respectively. Black squares are for UWB radar sensors.

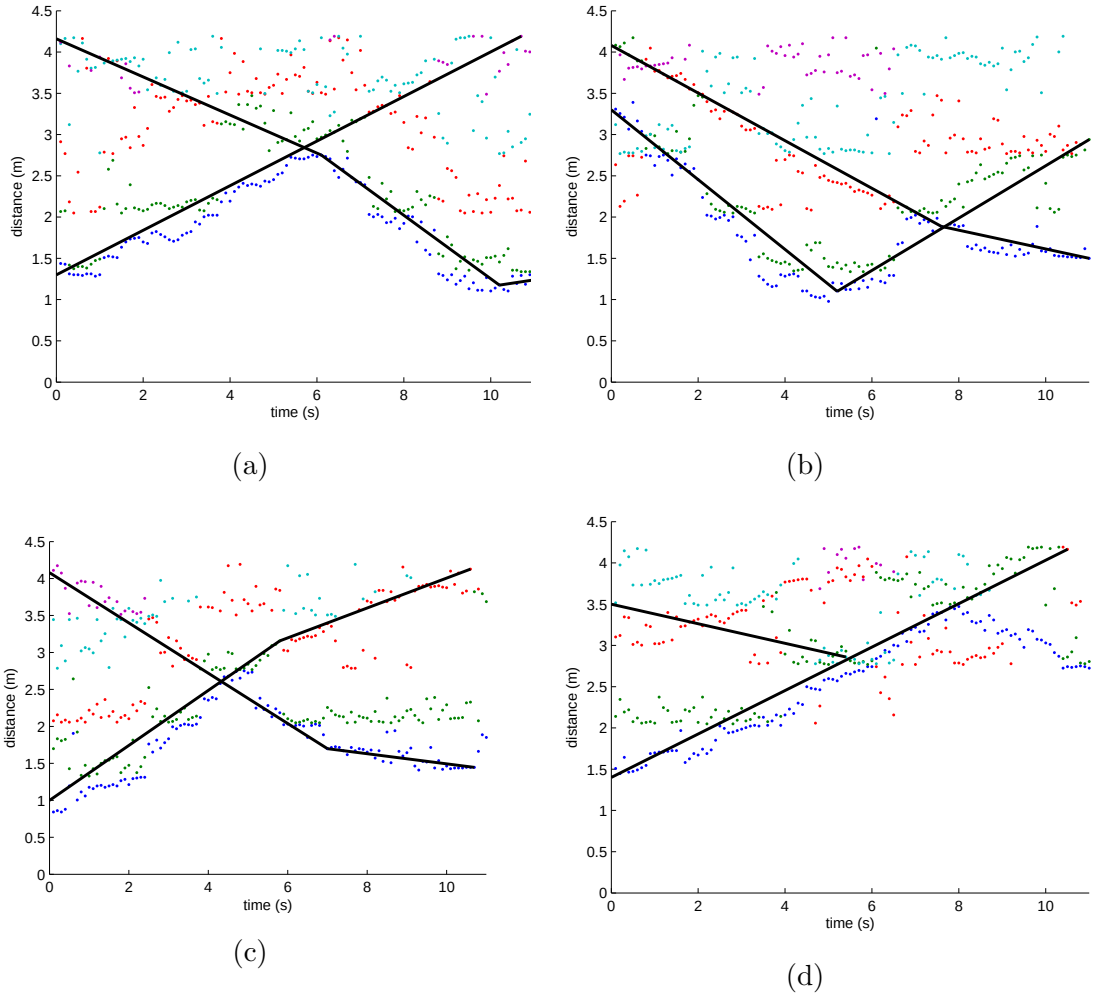

Figure 3.6: Multi-person tracking scenario, (Scenario-1). Range measurements of each sensor: (a) Sensor 1 (b) Sensor 2 (c) Sensor 3 (d) Sensor 4

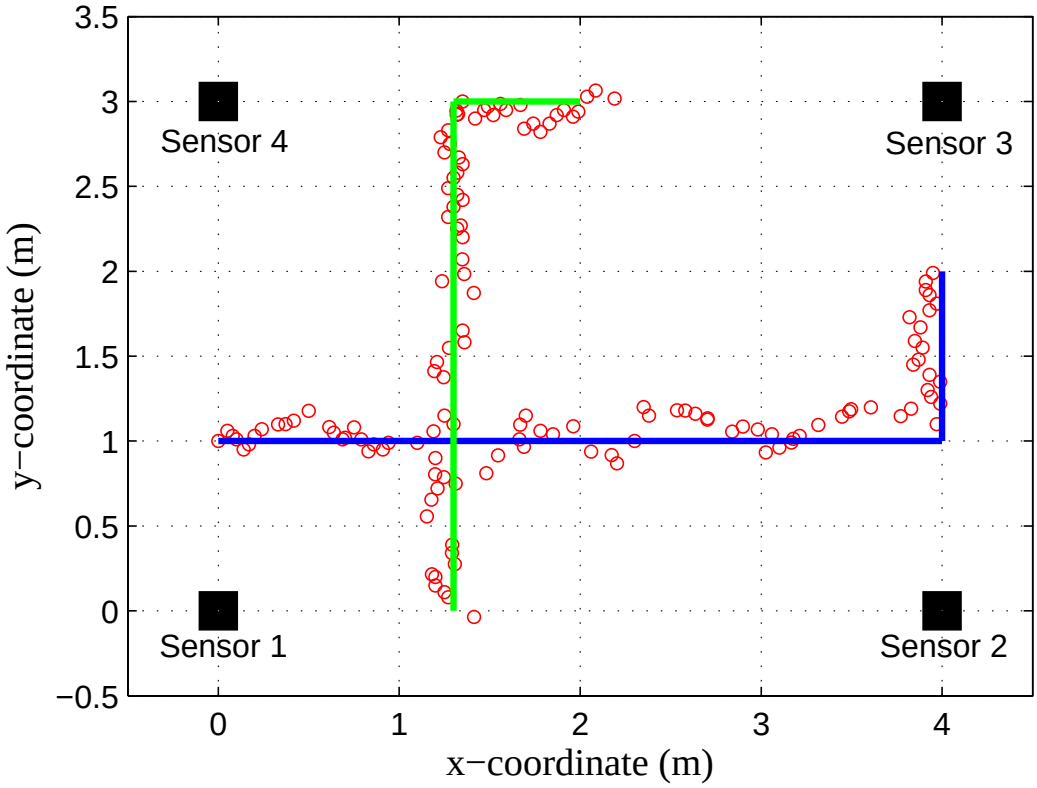

Figure 3.7: Scenario-2 for multiple person tracking. Green and blue solid lines denote the ground truth of the first and second person, respectively. Black squares are for UWB radar sensors.

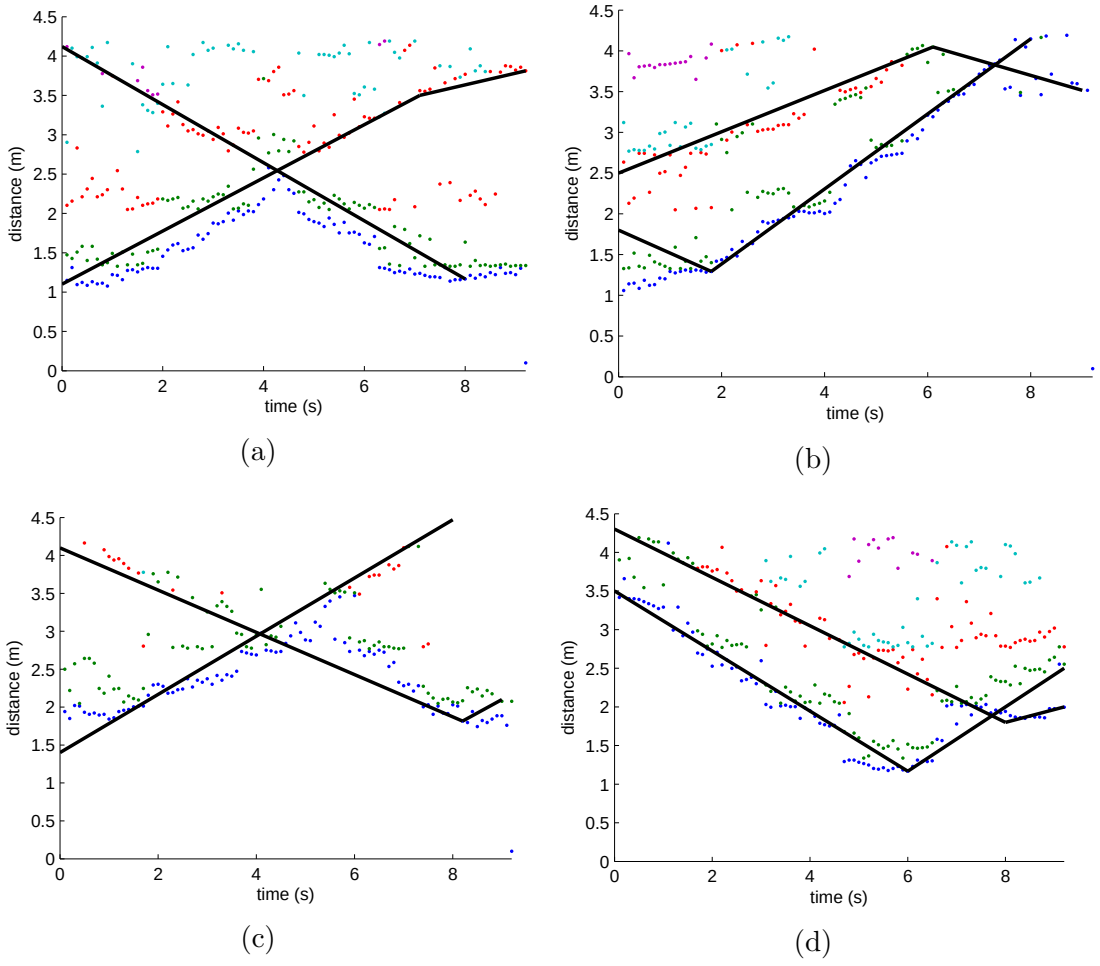

Figure 3.8: Multi-person tracking scenario, (Scenario-2). Range measurements of each sensor: (a) Sensor 1 (b) Sensor 2 (c) Sensor 3 (d) Sensor 4

The detection data of the sensors for the scenario in Figure 3.7 are shown in Figure 3.8. Processing the data is quite difficult in this case since there are many clutters and when the targets are closer to each other, they cannot be detected separately because of the occlusion problem. However, the proposed algorithm still provides accurate tracking in this challenging scenario.

Chapter 4

Conclusion

In this thesis, tracking of multiple persons has been performed in an indoor environment via UWB radar sensors. A detection algorithm has been proposed and GM-PHD filtering has been employed for accurate target tracking. GM-PDH filter overcomes the data association problem and achieves high tracking accuracy. A development kit from TimeDomain has been used to collect data in an office environment. Based on the data collection campaigns, the performance of the proposed algorithm has been evaluated and it has been shown that it can track single and multiple targets accurately in various scenarios. Future work involves the consideration of non-line-of-sight scenarios in multi-person tracking via UWB radar sensors.

Bibliography

[1] Z. Sahinoglu, S. Gezici, and I. Guvenc, *Ultra-Wideband Positioning Systems: Theoretical Limits, Ranging Algorithms, and Protocols*. Cambridge, U. K, 2008.

[2] http://www.timedomain.com/

[3] W. Dargie and C. Poellabauer, *Fundamentals of Wireless Sensor Networks: Theory and Practice*. John Wiley and Sons, 2010.

[4] K. Sohraby, D. Minoli, and T. Znati, *Wireless Sensor Networks: Technology, Protocols, and Applications*. John Wiley and Sons, 2007.

[5] J.-Y. Lee and R. Scholtz, "Ranging in a dense multipath environment using an UWB radio link," *IEEE J. Sel. Areas Commun.*, vol. 20, pp. 1677–1683, Dec 2002.

[6] M. Chiani and A. Giorgetti, "Coexistence between UWB and narrow-band wireless communication systems," *Proceedings of the IEEE*, vol. 97, pp. 231–254, Feb 2009.

[7] R. Zekevat and R. Buehrur, *Wireless Localization Using Ultra-Wideband Signals, 1st ed. New York, NY, USA*. Wiley-IEEE Press, 2012.

[8] D. Dardari, A. Conti, U. Ferner, A. Giorgetti, and M. Win, "Ranging with ultrawide bandwidth signals in multipath environments," *Proceedings of the IEEE*, vol. 97, pp. 404–426, Feb 2009.

[9] S. Gezici, Z. Tian, G. Giannakis, H. Kobayashi, A. Molisch, H. Poor, and Z. Sahinoglu, "Localization via ultra-wideband radios: a look at positioning aspects for future sensor networks," *IEEE Signal Processing Magazine*, vol. 22, pp. 70–84, July 2005.

[10] B. Sobhani, M. Mazzotti, E. Paolini, A. Giorgetti, and M. Chiani, "Effect of state space partitioning on bayesian tracking for UWB radar sensor networks," in *IEEE International Conference on Ultra-Wideband (ICUWB)*, pp. 120–125, Sep. 2013.

[11] B. Sobhani, E. Paolini, A. Giorgetti, M. Mazzotti, and M. Chiani, "Bayesian tracking in UWB radar sensor networks," in *IEEE International Conference on Communications Workshops (ICC)*, pp. 47–51, June 2013.

[12] S. Bartoletti, A. Conti, and A. Giorgetti, "Analysis of UWB radar sensor networks," in *IEEE International Conference on Communications (ICC)*, pp. 1–6, May 2010.

[13] M. Svecova, D. Kocur, R. Zetik, and J. Rovnakova, "Target localization by a multistatic UWB radar," in *20th International Conference on Radioelektronika (RADIOELEKTRONIKA)*, pp. 1–4, April 2010.

[14] X. wei Zhao, A. Gaugue, C. Liebe, J. Khamlichi, and M. Menard, "Through the wall detection and localization of a moving target with a bistatic UWB radar system," in *European Radar Conference (EuRAD)*, pp. 204–207, Sept 2010.

[15] G. Wei, Y. Zhou, and S. Wu, "Detection and localization of high speed moving targets using a short-range UWB impulse radar," in *IEEE Radar Conference (RADAR 2008)*, pp. 1–4, May 2008.

[16] D.-H. Kim, D.-W. Lim, L. Shen, H.-M. Kim, S.-C. Woo, and H. K. Yu, "Localization methods of multi-targets for UWB radar sensor networks," in *3rd International Asia-Pacific Conference on Synthetic Aperture Radar (APSAR)*, pp. 1–4, Sept 2011.

[17] H. Ding, C. Chen, S. Peng, X. Li, and L. Zheng, "Multistatic ultra-wideband localization for NLOS environments," in *Second International Conference on Intelligent System Design and Engineering Application (ISDEA)*, pp. 380–384, Jan 2012.

[18] S. Balckman and R. Popoli, *Design and Analysis of Modern Tracking Systems*. Norwood, MA, USA: Artech House, 2010.

[19] R. Mahler, *Statistical Multisource-Multitarget Information Fusion*. Artech House, 2007.

[20] R. Mahler, "Multitarget Bayes filtering via first-order multitarget moments," *IEEE Trans. Aerosp. Electron. Syst., vol. 39, no*, vol. 39, p. 11521178, Oct. 2003.

[21] M. S. Arulampalam, S. Maskell, N. Gordon, and T. Clapp, "A tutorial on particle filters for on-line nonlinear/non-Gaussian Bayesian tracking," in *IEEE Trans. Signal Process*, vol. 50, 2002.

[22] B. Ristic, S. Arulampalam, and N. Gordon, *Beyond the Kalman filter: Particle filters for tracking applications*. Artech House, 2007.

[23] F. Gustafsson, "Particle filter theory and practice with positioning applications," in *IEEE Aerosp. Electron. Syst. Mag.*, vol. 25, 2010.

[24] S. Jovanoska and R. Thoma, "Multiple target tracking by a distributed UWB sensor network based on the PHD filter," in *15th International Conference on Information Fusion (FUSION)*, pp. 1095–1102, July 2012.

[25] B. Sobhani, E. Paolini, A. Giorgetti, M. Mazzotti, and M. Chiani, "Target tracking for UWB multistatic radar sensor networks," *IEEE Journal of Selected Topics in Signal Processing*, vol. 8, pp. 125–136, Feb 2014.

[26] S. Jovanoska, R. Zetik, R. Thoma, F. Govaers, K. Wilds, and W. Koch, "Device-free indoor localization using a distributed network of autonomous UWB sensor nodes," in *Workshop on Sensor Data Fusion: Trends, Solutions, Applications (SDF), 2013*, pp. 1–6, Oct 2013.

[27] Y. Kilic, H. Wymeersch, A. Meijerink, M. Bentum, and W. Scanlon, "Device-free person detection and ranging in UWB networks," *IEEE Journal of Selected Topics in Signal Processing*, vol. 8, pp. 43–54, Feb 2014.

[28] Y. Zhou, C. L. Law, Y. L. Guan, and F. Chin, "Localization of passive target based on UWB backscattering range measurement," in *IEEE Int. Conf. on Ultra-Wideband (ICUWB)*, pp. 145–149, Sep. 2009.

[29] W.-K. Ma, B.-N. Vo, S. Singh, and A. Baddeley, "Tracking an unknown time-varying number of speakers using TDOA measurements: a random finite set approach," *IEEE Transactions on Signal Processing,*, vol. 54, pp. 3291–3304, Sept 2006.

[30] B.-N. Vo, S. Singh, and W.-K. Ma, "Tracking multiple speakers using random sets," in *IEEE International Conference on Acoustics, Speech, and Signal Processing (ICASSP)*, vol. 2, pp. ii–357–360, May 2004.

[31] J.-M. Valin, F. Michaud, and J. Rouat, "Robust 3D localization and tracking of sound sources using beamforming and particle filtering," in *IEEE International Conference on Acoustics, Speech and Signal Processing (ICASSP)*, vol. 4, pp. IV–IV, May 2006.

[32] First Report and Order 02-48, "Federal Communications Commissions," Feb. 2002.

[33] Y. Bar-Shalom, X. R. Li, and T. Kirubarajan, *Estimation with Applications to Tracking and Navigation*. John Wiley, 2001.

[34] B.-N. Vo and W.-K. Ma, "The Gaussian mixture probability hypothesis density filter," *IEEE Transactions on Signal Processing,*, vol. 54, pp. 4091–4104, Nov 2006.

[35] B. N. Vo, S. Singh, and A. Doucet, "Sequential Monte Carlo implementation of the PHD filter for multi-target tracking," *IEEE Trans. Aerosp. Electron. Syst., vol. 41, no*, vol. 41, no. 4, p. 12241245, 2005.

[36] B. Ristic, D. Clark, and B. Vo, "Improved SMC implementation of the PHD filter," 2010.

[37] E. Ozkan, M. B. Guldogan, U. Orguner, and F. Gustafsson, "Ground multiple target tracking with a network of acoustic sensor arrays using PHD and CPHD filters," *IEEE Int. Conf. Information Fusion (FUSION)*, 2011.

[38] M. B. Guldogan, U. Orguner, and F. Gustafsson, "Gaussian mixture PHD filter for multi-target tracking using passive Doppler-only measurements," in *9th IET Data Fusion Target Tracking Conference (DF TT 2012): Algorithms Applications*, pp. 1–6, May 2012.

[39] M. B. Guldogan, D. Lindgren, F. Gustafsson, H. Habberstad, and U. Orguner, "Multi-target tracking with PHD filter using Doppler-only measurements," *Digital Signal Process.*, vol. 27, pp. 1–11, April 2014.

[40] D. Clark, B. N. Vo, and J. Bell, "GM-PHD filter multitarget tracking in sonar images," in *SPIE Proc. SPIE Defense and Security Symposium*, 2006.

[41] M. Ulmke, O. Erdinc, and P. Willett, "GMTI tracking via Gaussian mixture cardinalized probability hypothesis density filter," *IEEE Trans. Aerosp. Electron. Syst.*, vol. 46, pp. 1821–1833, Oct. 2010.

[42] D. Laneuville and J. Houssineau, "Passive multi target tracking with GM-PHD filter," in *IEEE Int. Conf. Information Fusion (FUSION)*, 2010.

[43] R. Georgescu and P. Willett, "The GM-CPHD tracker applied to real and realistic multistatic sonar data sets," *IEEE Journal of Oceanic Engineering*, vol. 37, pp. 220–235, Apr. 2012.

[44] M. Pace, "Comparison of PHD based filters for the tracking of 3D aerial and naval scenarios," in *IEEE Radar Conference*, pp. 479–484, 2010.